Vol. 17, No. 3 (2018) 963-973
Revista Mexicana de Ingeniería Química

STRUCTURAL AND OPTICAL CHARACTERIZATION OF $(Fe_xMn_{1-x})_2O_3$ PIGMENTS FOR SOLAR ABSORPTION APPLICATIONS

CARACTERIZACIÓN ESTRUCTURAL Y ÓPTICA DE PIGMENTOS $(Fe_xMn_{1-x})_2O_3$ PARA APLICACIONES DE ABSORCIÓN SOLAR

E. Sánchez-Cruces[1], E. Barrera-Calva[1]*, L. Huerta Arcos[2], E. Ríos[3], F. González-García[1]
[1]*Departamento de Ingeniería de Procesos e Hidráulica, Universidad Autónoma Metropolitana-Iztapalapa, C.P 09340, Ciudad de México, México.*
[2]*Instituto de Investigación de Materiales, UNAM, Ciudad Universitaria, Av. Universidad 3000 Coyoacán, CDMX, C.P.04510c*
[3]*Posgrado en Ingeniería Agrícola y Uso Integral del Agua, Universidad Autónoma Chapingo, Carretera México-Texcoco, km. 38.5, Chapingo, Estado de México, C.P. 56230.*
Received: March 12, 2018; Accepted: June 6, 2018.

Abstract

In this research new materials are proposed to improve the capacity of solar energy absorption of solar thermal devices, such as distillers and flat plate solar collectors. The synthesis of a composite series of the system $(Fe_xMn_{1-x})_2O_3$ was proposed and its structural and optical properties were characterized. The crystal structure and optical properties were evaluated using X-ray diffraction and UV-Vis-IR spectroscopy techniques, respectively. To determine the relative concentration of hematite and bixbyite-type crystal phases as a function of the relative concentration of iron and manganese in the compounds, different refining analyzes were performed by the Rietveld method. X-ray photoelectron spectroscopy showed only the presence of trivalent metal species. The main results of analyzing the proposed system were: 1) the optimum manganese concentration and 2) solubility limits of Mn^{3+} and Fe^{3+} into the hematite and bixbyite structures, respective. The found values of solar absorbance (α_s) and thermal emission (ε_t) indicated that the addition of manganese is crucial for pigments performance used in solar absorption applications. The effects of the chemical composition on solar selectivity (α_s/ε_t) are discussed.

Keywords: pigments, bixbyite, hematite, Rietveld refinement, manganese.

Resumen

En esta investigación se proponen nuevos materiales para mejorar la capacidad de absorción de energía solar de dispositivos como destiladores y calentadores solares. Se propuso la síntesis de una serie compuesta del sistema $(Fe_xMn_{1-x})_2O_3$ y se caracterizaron sus propiedades estructurales y ópticas. La estructura cristalina y las propiedades ópticas se evaluaron usando difracción de rayos X y técnicas de espectroscopía UV-Vis-IR, respectivamente. Para determinar la concentración relativa de hematita y las fases de cristal de tipo bixbyita en función de la concentración relativa de hierro y manganeso en los compuestos, se realizaron distintos análisis de refinación por el método de Rietveld. La espectroscopía de fotoelectrones de rayos X demostró la presencia de especies de metales solo trivalentes. Los principales resultados obtenidos fueron: 1) la concentración óptima de manganeso y 2) límite de solubilidad. Los valores encontrados de absortancia (α) y emitancia térmica (ε) indicaron que la adición de manganeso es crucial para un buen rendimiento en aplicaciones de absorción solar. Se discuten los efectos de la composición química sobre la selectividad solar (α/ε).

Palabras clave: pigmentos, bixbyita, hematita, refinamiento Rietveld, manganeso

1 Introduction

Within the photothermal conversion of solar energy, it is essential the use of a type material called selective coatings that allow the optimum conversion of solar energy to thermal energy (Kennedy, 2002; Yianoulis *et al*. 2012). Selectivity term refers to the possibility of exploiting the effective decoupling between the incident solar spectrum (source) and the spectrum emitted by the system harnessing solar energy, usually a collector for heating water. For efficient photothermal conversion, solar selective surfaces must have high solar absorptance (α_s) and low thermal emittance (ε_t) at the operating temperature of the device using them (Cindrella,

* *Corresponding author. E-mail*: ebc@xanum.uam.mx
doi: 10.24275/uam/izt/dcbi/revmexingquim/2018v17n3/SanchezC
issn-e: 2395-8472

2007; Tiwari *et al*. 2016). Several authors have been studied and optimized different methods to obtaining selective coatings through selective paints (Geng *et al*., 2012; Ienei *et al*., 2010; Lundh *et al*., 2010; Ma *et al*., 2016; Orel *et al*., 2007; Tesfamichael *et al*., 2000; Wijewardane & Goswami, 2012). Paints are inexpensive, chemically resistant and easy to apply compared to the options offered by more sophisticated methods such as spray pyrolysis (Avila *et al*., 2004; Ienei *et al*., 2010), sol-gel (Kaluža *et al*. 2001; Vince *et al*., 2003), sputtering (Yin *et al*., 2009; Zhao & Wäckelgård, 2006) and evaporation, among others. (Mattox & Kominiak, 1975; Zhang & Mills, 1992).

A paint is a dispersion of solid particles (called pigments) suspended within a fluid, which after being applied as a thin layer on some substrate becomes a solid film. Pigments are responsible for providing color by absorption and reflection of light (Wijewardane & Goswami, 2012), different methods to obtain them have been investigated to achieve optimum values of absorptance. Iron oxides are commonly used as synthetic pigments in ceramics and porcelain materials because they can show a wide range of colors with a high staining power. The most chemically stable form of the different types of iron oxides is hematite (α-Fe_2O_3) (Cornell & Schwertmann, 2003), this property is added to other attributes like high corrosion resistance, low cost, non-toxicity and therefore low impact on environment. However, the red color of the hematite due to its electronic-structure properties makes it an unusable solar absorber pigment. A necessary, but not sufficient condition for a solar absorber material is be black for achieving full absorption of the visible part of the solar spectrum. Different oxides with more than two metal ions have been proposed as pigments, e.g. Tesfamichael proposed the oxide based on the system $FeMnCuO_x$ which give good absorption properties to coatings made by them (Tesfamichael *et al*., 2000). Bayón and collaborators have done several researches on thin films of copper-manganese oxides prepared by dip-coating method, achieving a solar absorptance value around 0.87 (Bayón *et al*., 2008a, 2008b; Bayón *et al*., 2010). In addition, pigment-based paints of $CuCrxMn(2\text{-}x)O_4$ (Geng *et al*. 2012), $CuCoMnO_x$ (El Mahallawy *et al*., 2014; He & Chen, 2015; L.Kaluza *et al*., 2001), $CuMn_2O_4$ (Ma *et al*., 2016) and $CuFeMnO_4$ (Kaluža *et al*. 2001) have also been studied, and the results showed that these oxides are competitive materials for use in selective coatings as solar absorbers. However, they may have serious disadvantages. For example, the use of cobalt nitrate precursor in those based in Co is not cost-effective because its relatively high price; additionally, some residues of Co could be toxic. Others, such as those based on $CuMnO_x$ spinel, exhibit low solar absorption, and only after the deposition of an antireflection layer, the multilayered sol-gel coatings may get competitive optical properties, although involving the use of more precursors and energy.

$(Fe_xMn_{1-x})_2O_3$ can be synthesized by the chemical precipitation method. This method is friendly with the environment and has some advantages such as the use of precursors of low cost, low energy consumption, few stages of synthesis, reactions may involve non-toxic products and does not require specialized equipment for mass production. $(Fe_xMn_{1-x})_2O_3$ system, at extreme compositions (x = 0 and 1) has different crystal structure. Fe_2O_3 (x = 1) corresponds to hematite (α-Fe_2O_3), its structure was determined by Pauling (Pauling & Hendricks, 1925), who found it crystallizes in, space group R-3c. The structure can be thought of as made of iron ions surrounded by six oxygen ions that are not in the corners of a regular octahedron. On the other hand, Mn_2O_3 (x = 0) crystallizes in bixbyite-type structure (α-Mn_2O_3) having space group Ia3.

The objective of this paper is to carry out the characterization of the structural and the optical properties, as well as the assessment of the chemical composition of a series of compounds of $(Fe_xMn_{1-x})_2O_3$ system (x = 0, 0.35, 0.4, 0.5, 0.8, 0.85 0,87 ,0.9, 0.93 ,1) synthesized by the chemical precipitation method. The effect of the composition on the optical properties of the pigments was analyzed to evaluate their potential application as solar absorbers.

2 Experimental

2.1 Synthesis of $(Fe_xMn_{1-x})_2O_3$

For the synthesis of the iron- manganese oxides, raw materials used were $MnCl_2$ $4H_2O$, (97%, Sigma-Aldrich) and $FeCl_3$-$6H_2O$ (97%, Sigma-Aldrich). The appropriate quantities of $MnCl_2$ $4H_2O$ and $FeCl_3$-$6H_2O$ were dissolved in deionized water, per each sample. The two solutions were mixed in appropriate amount to get the desired Fe/Mn molar concentration. The mixture was precipitated using a concentrated NH_4OH solution (28%, Sigma-Aldrich) under stirring. During the entire precipitation process, the pH was maintained above 11. The resulting precipitate was

washed three times with distilled water dried at ambient temperature and calcined at 800 °C for 1 h.

2.2 *Characterization of materials*

The X-ray diffractograms of the powders were measured in a Bruker D-8 advance diffractometer fitted with a Cu X-ray tube and a one-dimensional position-sensitive silicon strip detector (Bruker, Lynxeye). The diffraction intensity as a function of 2θ angle was measured between 20° and 70°, with a 2θ step 0.020415°, for 192 s per point. Crystalline structures were refined using the Rietveld method (Rietveld, 1969), as implemented in the Fullprof Suite Program version 3.00 (Rodriguez-Carvajal, 2003; Rodríguez-Carvajal, 1990). In order to parameterize refinements, were used THC pseudo-Voigt profile for modeling peak shape (Thompson *et al*., 1987). Refined parameters include those associated with the size of the unit cell, the crystallite size and the relative concentration (wt%) of the phases present in the sample, among others.

X-ray photoelectron spectroscopy (XPS) analysis was performed in several selected samples using ultra-high vacuum (UHV) system Scanning XPS microprobe PHI 5000 VersaProbe II, with a Al K_α X-ray source ($h\nu$= 1486.6 eV) monochromatic with 100 μm beam diameter, and a MCD analyzer. The XPS spectra were obtained at 45º to the normal surface in the constant pass energy (CAE) E_0 = 117.40 and 11.75 eV for survey surface and high-resolution narrow scan. The surface samples were etched for 8 min with 1 kV Ar^+ at 0.25 $\mu A/mm^2$. The binding energies were corrected for the charge shift using the silver $3d_{5/2}$ photo peak at 368.20 eV, having a FWHM of 0.56 eV, and C 1s hydrocarbon groups at 285.00 eV, Au $4f_{7/2}$ in 84.00 eV central peak core level position. The XPS deconvolution analysis of spectra was fitted with the programs PHI Multipack© version 9.6.0.15 and SDP© v 4.1. The associated uncertainty of the binding energy of the deconvolution of the central peak was about 5% (± 0.05 eV) and a chi-square value for the adjustment of less than 1.5.

The spectral reflectance of the compounds was measured in the range of 0.3 μm to 20 μm. The optical characterization on this wide range, was carried out in a Cary 5E Varian spectrophotometer, equipped with an integrating sphere to record the reflectance of wavelengths from 0.3 μm to 2.5 μm, as well as in a iS50 FTIR spectrophotometer.

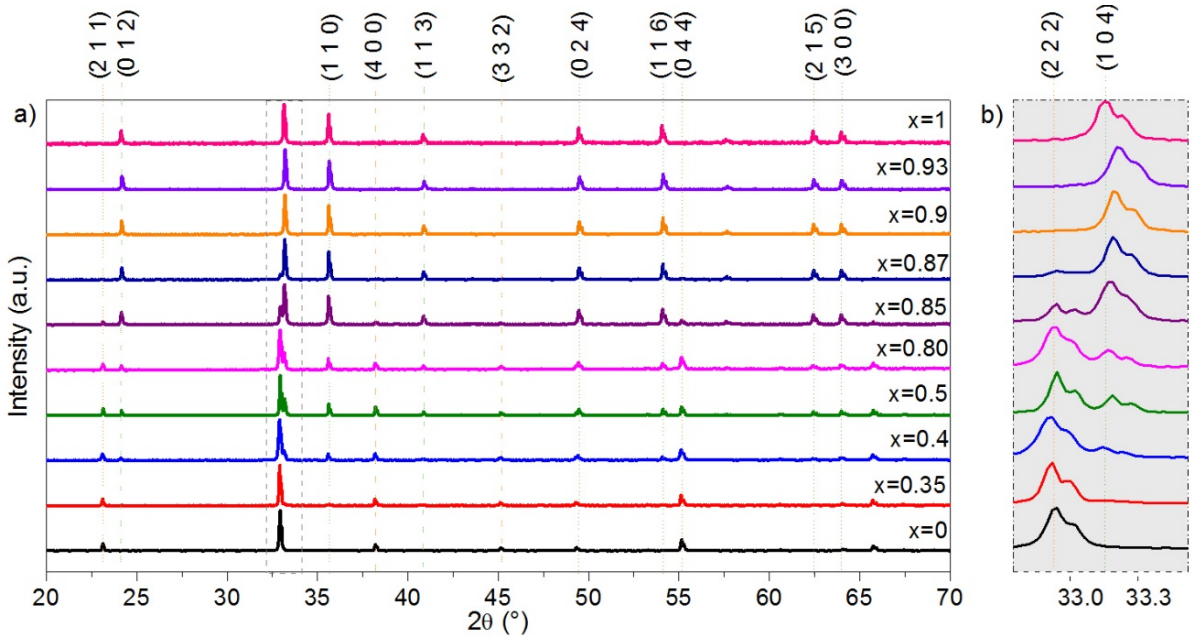

Fig. 1. X-ray diffraction patterns of the all samples calcined at 800 ° C for 1h (a). Zoom of the 2θ range between 32.7° and 34.5° (b).

3 Results and discussion

3.1 Structural analysis of Fe-Mn oxides

Figure 1 (a) shows X-ray diffractograms of all synthesized samples. The crystalline phases present in these samples are isostructural to the α-Fe_2O_3 (PDF 01-087-1165) for compositions with x=1.00, 0.93 and 0.90; in addition to α-Fe_2O_3, the bixbyite-type phase isostructural to the α-Mn_2O_3 (PDF 00-041-1442) is present for samples with composition x=0.87, 0.85, 0.80, 0.50, 0.40, 0.35). Sample not containing Fe (x=0) presents only bixbyite-type phase. In Fig. 1 (b) is plotted the 2θ range of X-ray patterns of all samples between 32° and 34°, where it is clearly seen the gradual crystalline phase change of the compounds. Within this 2θ range, the most representative Bragg reflections of the hematite and bixbyite phases, (104) and (222), respectively, appear. As it is observed, the reflection (104) presents a slight shifting to higher 2θ values, which may be attributed to the incorporation of Mn^{3+} cations in the hematite structure. This subtle shifting to higher 2θ values corresponds to a decrease in the size of the crystal cell, which is in some way unexpected, since in a six-coordination, as that corresponding to the metal cation in the hematite structure, the ionic radii of Fe^{3+} and Mn^{3+} are, according to Shannon (Shannon, 1976), the same and in the order to 0.645 Å. In our opinion, this fact reflects the small differences in the distribution of electrons of Fe^{3+} and Mn^{3+}.

The crystallographic data for the α-Fe_2O_3 and α-Mn_2O_3 have been reported by Maslen (Maslen *et al.*, 1994) and Geller (Geller, 1971a); thus, performing Rietveld refinement analysis, it is possible to determine in a quantitative way the effect of composition on the cell parameters, as well as the concentration (wt%) of both crystalline phase present in each compound. The unit cell of hematite was modeled with the hexagonal setting of the rhombohedral symmetry described by the space group R-3c (167), and a basis containing one Fe^{3+} at the relative coordinates $(0,0,z)$ and one O^{2-} at the relative coordinates $(x,0,1/4)$; the initial values for z and x were as those reported in (Maslen *et al.*, 1994). On the other hand, the unit cell of bixbyite-type structure of Mn_2O_3 was modeled with the cubic symmetry described by the space group Ia-3, a nd basis containing two Mn^{2+} at the relative coordinates $(0,0,0)$ and $(x,0,z)$ and an O^{2-} at coordinates (x,y,z). All initial values for the variable relative coordinates were as those reported in (Geller, 1971b).

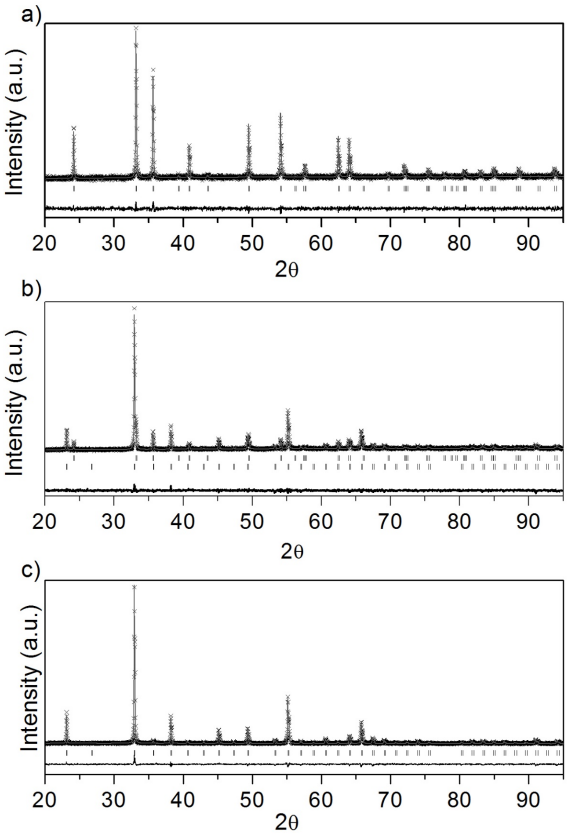

Fig. 2. Rietveld refinement plots of the samples a) x=1, b) x=0.5, c) x=0. The scatter points and the upper solid line correspond to the experimental and calculated data, respectively. The lower solid line is the difference between them. The marks on the bottom correspond to a) hematite, b) hematite (upper marks) and bixbyite (lower marks) and c) bixbyite.

In order to show the agreement between the experimental X-ray diffractograms and the calculated ones, typical Rietveld refinement plots are depicted in Fig. 2; they correspond to the samples with x=1.0, x=0.5 and x=0.0. Table 1 shows the lattice parameters and the concentration in wt% obtained from the Rietveld refinement analyses of the series compounds $(Fe_xMn_{1-x})_2O_3$.

3.2 X-Ray photoelectron spectroscopy (XPS)

Since Fe and Mn possess different oxidation states, which could significantly impact the optical properties of the compounds, X-ray photoelectron spectroscopy (XPS) was used for analyzing the film composition and confirms the valence state of the metals, of some representative compounds.

Table 1. Crystallographic data of each synthesized sample obtained from the Rietveld refinement of the XRD results for the substitutional solid solution $(Fe_xMn_{1-x})_2O_3$.

Sample	Lattice parameters					wt (%)	
	Fe_2O_3			Mn_2O_3			
	a=b (Å)	c (Å)	Crystal size (nm)	a=b=c (Å)	Crystal size (nm)	Fe_2O_3	Mn_2O_3
x=1	5.03566(4)	13.74760(14)	155(2)	–	–	100	–
x=0.93	5.03681(3)	13.73867(12)	182(3)	–	–	100	–
x=0.9	5.03666(3)	13.73557(11)	226(4)	–	–	100	–
x=0.87	5.03616(3)	13.73849(11)	217(3)	9.41470(23)	638(55)	95.2(1)	4.8(1)
x=0.85	5.03596(8)	3.73717(29)	158(2)	9.41197(20)	405(30)	85.0(2)	14.5(2)
x=0.8	5.03697(5)	13.73273(18)	234(10)	9.41246(9)	157(3)	35.9(1)	64.1(3)
x=0.5	5.03780(7)	13.73591(28)	200(10)	9.41390(9)	200(10)	21.3(6)	78.7(3)
x=0.4	5.03729(7)	13.73161(27)	212(14)	9.41263(11)	114(2)	21.4(6)	78.6(3)
x=0.35	5.03953(20)	13.72692(62)	262(76)	9.41518(6)	270(9)	6.9(3)	93.1(3)
x=0	–	–	–	9.41238(6)	176(2)	–	100

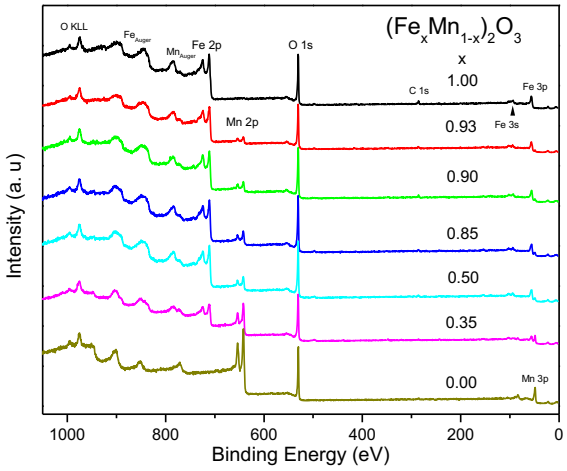

Fig. 3. XPS wide survey spectra of $(Fe_xMn_{1-x})_2O_3$ system with x = 0, 0.35, 0.4, 0.5, 0.8, 0.85 0,87 ,0.9, 0.93, and 1.00 samples.

Survey spectra of all the measured samples are shown at figure 3, where some differences between samples are ascribed to the different molar relation each one. For a quantitative analysis, samples of nominal composition x = 1 (Fe_2O_3) and x = 0 (Mn_2O_3) were used as references. For the iron oxide the analyzed lines were associated to Fe_2p (710.9 eV) and O 1s (531 eV), and for the manganese oxide Mn_2p (541 eV) and O 1s (531eV), as has been shown by Yamashita and Ali Audi (Yamasshita and Hayes, 2006) and (Audi and Sherwood , 2002).

Table 2. Quantitative XPS analyses for oxides Fe-Mn.

Sample	Fe % at	Mn % at	O % at
x=1	40	0	60
x=0.93	33.1	5.3	61.6
x=0.9	32.6	6.5	60.8
x=0.85	31.2	7.5	61.3
x=0.5	31.9	7.4	60.7
x=0.35	19.8	22.4	58.4
x=0	0	40	60

Once using a XPS deconvolution analysis of the samples spectra, the atomic percentages of iron, manganese and oxygen of each sample analyzed were estimated and summarize at table 2. For these analyses the peaks corresponding to the orbital Mn_2p and Fe_2p were used. Figures 4 and 5, show this peak only for some representative samples with different Mn/Fe molar composition. The spectra were normalized to be analyzed in a better way. From the data in Table 2, except for the sample with x = 0.5, it is observed that the change in the at % concentration of the elements, within the experimental uncertainty, is in accordance with the nominal composition.

XPS technique also provided information about the oxidation state of the iron and manganese ions. To establish the presence or not, of different valence states of Fe and Mn, the Fe_2p and Mn_2p peak analysis deconvolution was performed.

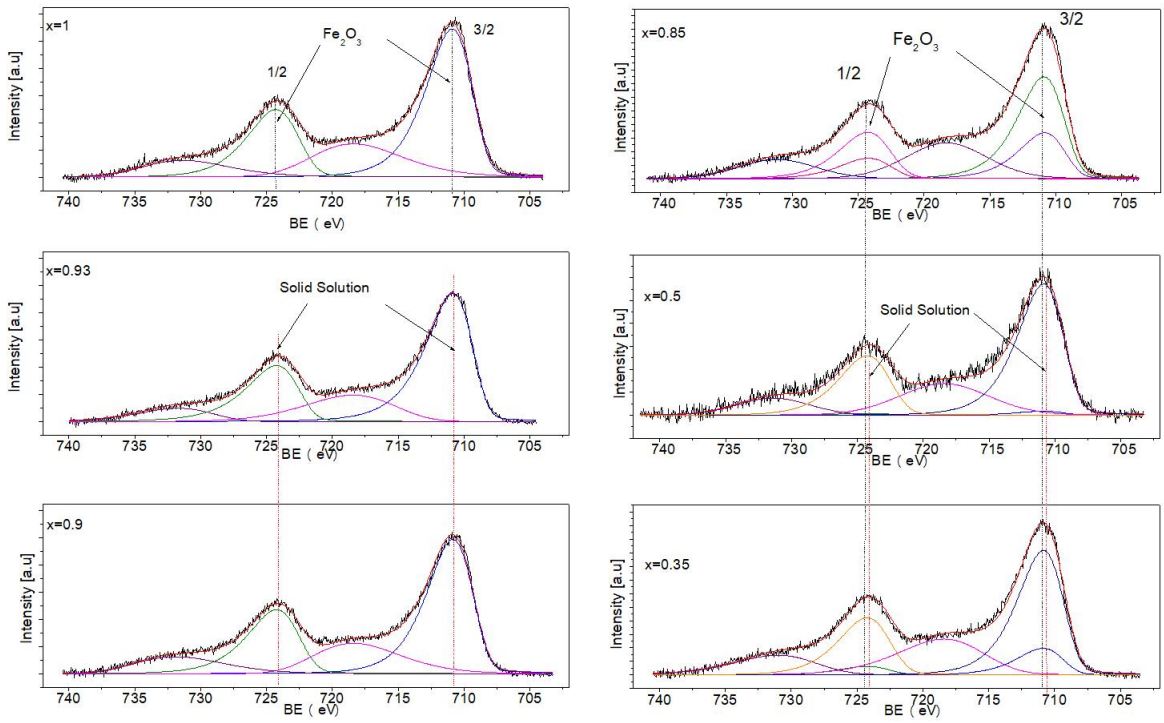

Fig. 4. Deconvolution of the Fe2p peak corresponding to iron-manganese oxide samples annealed at 800°C.

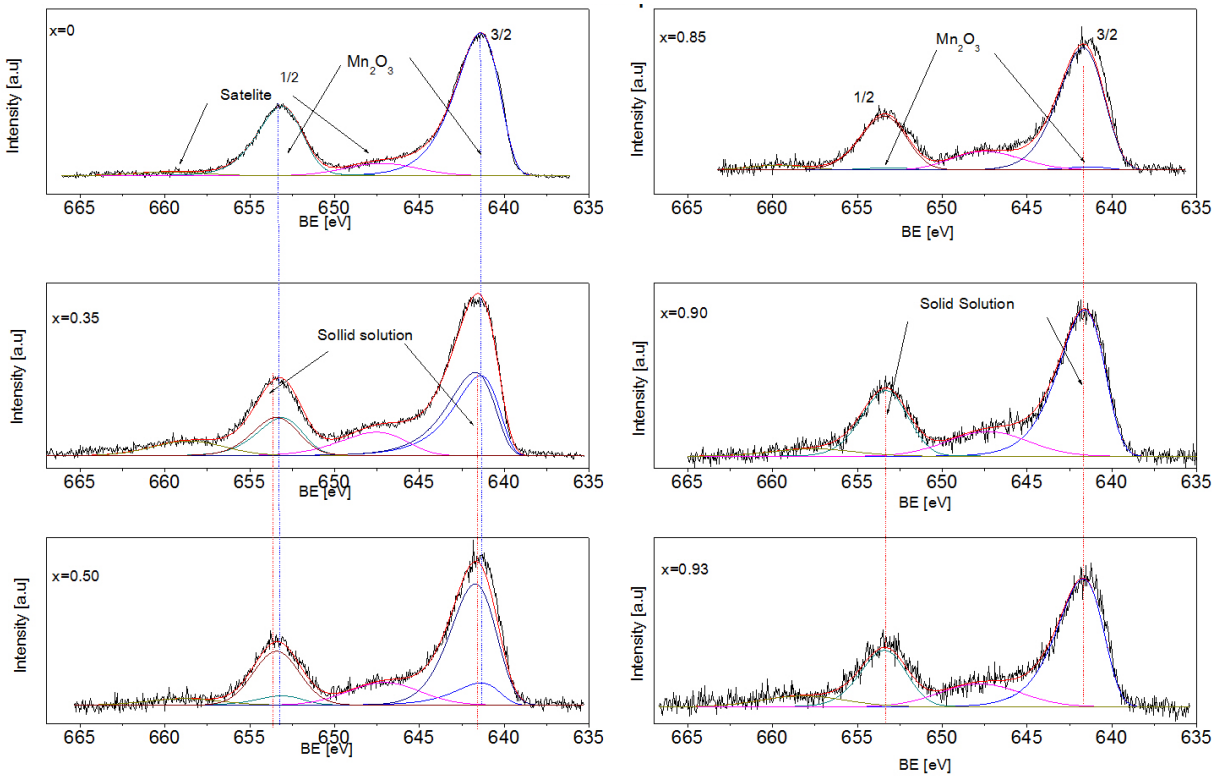

Fig. 5. Deconvolution of the Mn 2p peak corresponding to iron-manganese oxide samples annealed at 800°C

The Fe_2p peak in Fig. 4 showed only two components: one at 710.9 eV associated with Fe^{3+} in α-Fe_2O_3 and another at 710.85 eV associated with Fe^{3+} in α-Fe_2O_3-Mn_2O_3 solid solution.

In a similar way, the Mn_2p peak in Fig. 5 presents only two components: one at 641.51 eV associated with Mn^{3+} in Mn_2O_3 and another at 641.67 eV associated with Mn^{3+} in a Fe_2O_3-Mn_2O_3 solid solution. These results support the presence of only Fe^{3+} and Mn^{3+} in our compounds.

It has been reported that the binding energy for the Mn_2p peak of Mn^{2+} in manganese ferrites is 640.2 eV (Gillot *et al*., 1999). Despite we used a Mn_2+ precursor for the synthesis of the compounds; we did not detect the presence of divalent manganese. This fact is in agreement with the results reported by Bayón (2008). These authors also did not find the presence of Mn^{2+} in thin films of copper-manganese oxide annealed at 500 °C, which may be due to the oxidation during the synthesis or the calcination processes.

3.3 Optical properties of the compounds

With the aim of determining the absorption features of the compounds for their application as selective absorbers, reflectance spectra in the UV/Vis/NIR (0.25 μm-2.5 μm) regions were recorded. These spectra are depicted in Fig. 6. The reflectance values are less than 7.5% for all pigments, with the exception of sample with x = 1. The sudden increase in reflectance of this sample agrees with the characteristic red color of the hematite. On the other hand, in the NIR region the reflectance increases in all samples as wavelength increases.

The resulting solar absorptances were calculated, in the visible region of the spectra. In fact, although a low reflectance in the UV-Vis region is the main reason for increasing the solar absorptance (Bayón *et al*., 2008), the NIR region also has some influence in its value. From the spectra of Fig.6, it is easy to calculate the solar absorptance (Duffie & Beckman, 2013). Theoretically, this parameter is recognized, as the fraction of the incident radiation of wavelength λ that is absorbed by the surface, when the radiation source is the sun. It was calculated according to equation 1, where λ is wavelength, $R(\lambda)$ reflectance and Is (λ) normal irradiance of the sun.

$$\alpha_s = \frac{\int_{0.3}^{2.5} I_s(\lambda)(1-R(\lambda))d\lambda}{\int_{0.3}^{2.5} I_s(\lambda)d\lambda} \qquad (1)$$

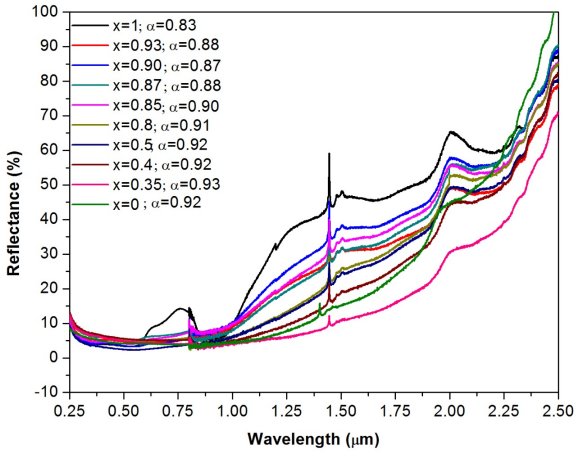

Fig. 6. UV/Vis/NIR reflectance spectra of the 800°C annealed $(Fe_xMn_{1-x})_2O_3$.

According to the results of calculating the solar absorptance, from reflectance spectra, shown in the Fig. 6, the lowest solar absorptance resultant is around 0.83, which are low values considering their use as solar absorbers, it is evident that the highest values of solar absorptance are present in the compounds having higher absorption values in the NIR region. It was possible to decrease the reflectance in this region and hence to improve the absorptance when iron ions were replaced by manganese, in all cases the absorptance was gradually increasing. The most absorbing pigment (α_s = 0.93), which correspond to the x=0.35 sample it is a value similar to the absorptance of selective paints obtained with pigments that do not contain iron (Ma. Geng *et al*., 2016).

The influence of the thermal emittance of the pigments on the solar thermal application it is very important, it is useful to remember that the emittance is a property of the material and depends strongly on the surface condition of the material, but the calculation of emittance of powders can give an overview of the behavior of a complete system when using these pigments on solar energy applications.

The thermal emittance is a ratio between a radiation emitted by the surface and the radiation that a black body at the same temperature emit, which is presented as:

$$\varepsilon_T = \frac{\int_{2.5}^{25} E(\lambda,T)(1-R(\lambda))d\lambda}{\int_{2.5}^{25} E(\lambda,T)d\lambda} \qquad (2)$$

Where $E(\lambda,T)$ is the spectrum of the radiation of a blackbody at temperature T.

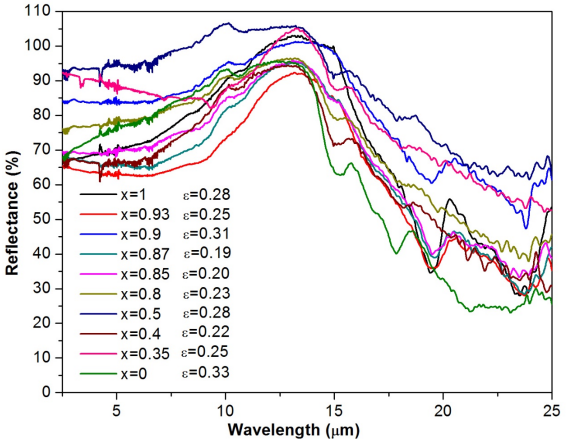

Fig. 7. The reflectance spectra in the range from 2.5 to 25 μm and the corresponding thermal emittance (ε_{50}) of the pigments annealed at 800°C.

The measured IR reflectance spectra of each sample and the calculated thermal emittance, by means equation 2, are presented in Fig. 7. Each one of the powders calcined at 800°C has a different spectrum, in different works it has been observed that factors like the perfection of the crystal, integration of impurities and different cooling rates cause a non-systematic rise of the emittance at different temperatures, the changes in the emittance values shown in Fig.7 can be explained by incorporation of Mn ions into the system.

Conclusions

In this research, FeMnO pigments were synthesized successfully using a straightforward and economical method. The XRD results revealed that annealed pigments at 800 °C were composed of a crystalline phases Fe_2O_3 and Mn_2O_3, however, a few samples were composed of both, as solid solution or phases segregations. The solid solution remained until x = 0.35, then, it disappears when x = 0.40 (manganese 40% and iron 60%), it was concluded that this result represents the solubility limit of $(Fe_xMn_{1-x})_2O_3$ system. Through the XPS measurements, only one oxidation state (3+) was identified for the metals present (Fe and Mn) in the system. When the manganese concentration was increased, the value of the solar absorptance also increased. The results indicated that the best selectivity values, S, were obtained in the sample x = 0.35, where the values, solar absorptance (α_s) and thermal emittance (ε_t) were 0.93 and 0.25, respectively, leading to a good S=3.8. The above results represent the desirable values of solar optical properties of pigments to be used as efficient solar selective materials. In general, it is concluded that the manganese aggregation in the iron oxide pigments improve the solar absorptance to be used in different solar collectors, like solar stills, solar stoves, solar drier and flat plate solar collectors.

Nomenclature

E spectrum of the radiation of a blackbody at temperature T
Is normal irradiance of the sun
R reflectance
T temperature

Greek symbols
α solar absorptance
ε thermal emittance
λ wavelength

Acknowledgments

Elisa Sánchez acknowledge UAM (México) for financial support to get a Doctorate studies scholarship.

References

Ali Audi, A. & Sherwood P.M.A, (2002). Valence band X ray photoelectron spectroscopies studies of manganese and its oxide interpreted by cluster and band structure calculations. *Surface and Interface Analysis 33*, 274-282

Avila G. A., Barrera C. E., Huerta A., L., & Muhl, S. (2004). Cobalt oxide films for solar selective surfaces, obtained by spray pyrolisis. *Solar Energy Materials and Solar Cells 82*, 269-278. https://doi.org/10.1016/j.solmat.2004.01.024

Bayón, R., San Vicente, G., Maffiotte, C., & Morales, Á. (2008a). Characterization of copper-manganese-oxide thin films deposited by dip-coating. *Solar Energy Materials and Solar Cells 92*, 1211-1216. https://doi.org/10.1016/j.solmat.2008.04.011

Bayón, R., San Vicente, G., Maffiotte, C., & Morales, Á. (2008b). Preparation of selective absorbers based on CuMn spinels by dip-coating method. *Renewable Energy 33*, 348-353. https://doi.org/10.1016/j.renene.2007.05.017

Bayón, R., San Vicente, G., & Morales, Á. (2010). Durability tests and up-scaling of selective absorbers based on copper-manganese oxide deposited by dip-coating. *Solar Energy Materials and Solar Cells 94*, 998-1004. https://doi.org/10.1016/j.solmat.2010.02.006

Cindrella, L. (2007). The real utility ranges of the solar selective coatings. *Solar Energy Materials and Solar Cells 91*, 1898-1901. https://doi.org/10.1016/j.solmat.2007.07.006

Cornell, R. M., & Schwertmann, U. (2003). *The Iron Oxides: Structure, Properties, Reactions, Occurrences and Uses*. Wiley. https://doi.org/10.1002/3527602097

Duffie, J. A., & Beckman, W. A. (2013). *Solar Engineering of Thermal Processes: Fourth Edition. Solar Engineering of Thermal Processes*. Fourth edition. https://doi.org/10.1002/9781118671603

El Mahallawy, N., Shoeib, M., & Ali, Y. (2014). Application of CuCoMnOx coat by sol gel technique on aluminum and copper substrates for solar absorber application. *Journal of Coatings Technology and Research 11*, 979-991. https://doi.org/10.1007/s11998-014-9592-9

Geller, S. (1971a). Structure of α-Mn_2O_3, $(Mn_{0.983}Fe_{0.017})_2O_3$ and $(Mn_{0.37}Fe_{0.63})_2O_3$ and relation to magnetic ordering. *Acta Crystallographica Section B Structural Crystallography and Crystal Chemistry 27*, 821-828. https://doi.org/10.1107/S0567740871002966

Geller, S. (1971b). Structure of α-Mn_2O_3, $(Mn_{0.983}Fe_{0.017})_2O_3$ and $(Mn_{0.37}Fe_{0.63})_2O_3$ and relation to magnetic ordering. *Acta Crystallographica Section B Structural Crystallography and Crystal Chemistry 27*, 821-828. https://doi.org/10.1107/S0567740871002966

Geng, Q., Zhao, X., Gao, X., Yu, H., Yang, S., & Liu, G. (2012). Optimization design of CuCr xMn_2-xO_4-based paint coatings used for solar selective applications. *Solar Energy Materials and Solar Cells 105*, 293-301. https://doi.org/10.1016/j.solmat.2012.06.033

Gillot, B., Buguet, S., Kester, E., Baubet, C., & Tailhades, P. (1999). Cation valencies and distribution in the spinels Co_x Cu_y Mn z Fe u $O_4 + \delta$ ($\delta \geq 0$) thin films studied by X-ray photoelectron spectroscopy. *Thin Solid Films 357*, 223-231. https://doi.org/10.1016/S0040-6090(99)00402-2

He, M., & Chen, R. (2015). Structural and optical properties of CuMnCoOx spinel thin films prepared by a citric acid-based sol-gel dip coating route for solar absorber applications. *Journal of Sol-Gel Science and Technology 74*, 528-536. https://doi.org/10.1007/s10971-015-3630-7

Ienei, E., Isac, L., Cazan, C., & Duta, A. (2010). Characterization of $Al/Al_2O_3/NiOx$ solar absorber obtained by spray pyrolysis. *Solid State Sciences 12*, 1894-1897. https://doi.org/10.1016/j.solidstatesciences.2010.05.028

Kaluža, L., Šurca-Vuk, A., Orel, B., Dražič, G., & Pelicon, P. (2001). Structural and IR spectroscopic analysis of sol-gel processed $CuFeMnO_4$ spinel and $CuFeMnO_4$/silica films for solar absorbers. *Journal of Sol-Gel Science and Technology 20*, 61-83. https://doi.org/10.1023/A:1008728717617

Kennedy, C. (2002). Review of mid-to high-temperature solar selective absorber materials. *NREL Technical Report*. https://doi.org/10.2172/15000706

Kaluza, L. Orel B., Drazic, G. & Kohl, M. (2001). Sol-gel derived CuCoMnOx spinel coatings for solar absorbers: Structural and optical properties. *Solar Energy Materials & Solar Cell 70*, 187-201. https://doi.org/10.1016/S0927-0248(01)00024-1

Lundh, M., Blom, T., & Wäckelgård, E. (2010). Antireflection treatment of Thickness Sensitive Spectrally Selective (TSSS) paints for thermal solar absorbers. *Solar Energy 84*, 124-129. https://doi.org/10.1016/j.solener.2009.10.016

Ma, P., Geng, Q., Gao, X., Yang, S., & Liu, G. (2016). Solution combustion of spinel $CuMn_2O_4$

ceramic pigments for thickness sensitive spectrally selective (TSSS) paint coatings. *Ceramics International 42*, 11966-11973. https://doi.org/10.1016/j.ceramint.2016.04.122

Maslen, E. N., Streltsov, V. a., Streltsova, N. R., & Ishizawa, N. (1994). Synchrotron X-ray study of the electron density in α-Fe_2O_3. *Acta Crystallographica B50*, 435-441. https://doi.org/10.1107/S0108768194002284

Mattox, D. M., & Kominiak, G. J. (1975). Deposition of semiconductor films with high solar absorptivity. *Journal of Vacuum Science and Technology 12*, 182. https://doi.org/10.1116/1.568750

Orel, B., Spreizer, H., Slemenik Perše, L., Fir, M., Šurca Vuk, A., Merlini, D., ... Köhl, M. (2007). Silicone-based thickness insensitive spectrally selective (TISS) paints as selective paint coatings for coloured solar absorbers (Part I). *Solar Energy Materials and Solar Cells 91*, 93-107. https://doi.org/10.1016/j.solmat.2006.07.013

Pauling, L., & Hendricks, S. B. (1925). The crystal structures of hematite and corundum. *Journal of the American Chemical Society 47*, 781-790. https://doi.org/10.1021/ja01680a027

Rietveld, H. M. (1969). A profile refinement method for nuclear and magnetic structures. *Journal of Applied Crystallography 2*, 65-71. https://doi.org/10.1107/S0021889869006558

Rodriguez-Carvajal, J. (2003). Fullprof suite. LLB Sacley and LCSIM Rennes. France.

Rodríguez-Carvajal, J. (1990). FullProf: A program for rietveld refinement and pattern matching analysis. Satellite Meeting on Powder Diffraction of the XV Congress of the IUCr, Toulouse, France.

Shannon, R. D. (1976). Revised effective ionic radii and systematic studies of interatomic distances in halides and chalcogenides. *Acta Crystallographica Section A32*, 751-767. https://doi.org/10.1107/S0567739476001551

Tesfamichael, T., Hoel, A., Wkelgrd, E., Niklasson, G. A., Gunde, M. K., & Orel, Z. C. (2000). Optical characterization and modeling of black pigments used in thickness-sensitive solar-selective absorbing paints. *Solar Energy 69*, 35-43. https://doi.org/10.1016/S0038-092X(01)00016-0

Thompson, P., Cox, D. E., & Hastings, J. B. (1987). Rietveld refinement of Debye-Scherrer synchrotron X-ray data from Al_2O_3. *Journal of Applied Crystallography 20*, 79-83. https://doi.org/10.1107/S0021889887087090

Tiwari, G. N., Tiwari, A., & Shyam. (2016). Flat-plate collectors. In *Handbook of Solar Energy* (pp. 171-246). https://doi.org/10.1007/978-981-10-0807-8_5

Vince, J., Šurca Vuk, A., Opara Krašovec, U., Orel, B., Köhl, M., & Heck, M. (2003). Solar absorber coatings based on CoCuMnOx spinels prepared via the sol-gel process: Structural and optical properties. *Solar Energy Materials and Solar Cells 79*, 313-330. https://doi.org/10.1016/S0927-0248(02)00457-9

Wijewardane, S., & Goswami, D. Y. (2012). A review on surface control of thermal radiation by paints and coatings for new energy applications. *Renewable and Sustainable Energy Reviews 16*, 1863-1873. https://doi.org/10.1016/j.rser.2012.01.046

Yamashita T. & Hayes P. (2008). Analysis of XPS of Fe^{+2} and Fe^{+3} ions in oxide materials. *Applied Surface Science 254*, 2441-2449.

Yianoulis, P., Giannouli, M., & Kalogirou, S. A. (2012). 3.09 - Solar selective coatings. *Comprehensive Renewable Energy 3*, 301-312. http://dx.doi.org/10.1016/B978-0-08-087872-0.00309-7

Yin, Y., Pan, Y., Hang, L. X., McKenzie, D. R., & Bilek, M. M. M. (2009). Direct current reactive sputtering Cr-Cr_2O_3 cermet solar selective surfaces for solar hot water applications. *Thin Solid Films 517*, 1601-1606. https://doi.org/10.1016/j.tsf.2008.09.082

Zhang, Q. C., & Mills, D. R. (1992). High solar performance selective surface using bi-sublayer cermet film structures. *Solar Energy Materials and Solar Cells 27*, 273-290. https://doi.org/10.1016/0927-0248(92)90089-8

Zhao, S., & Wäckelgård, E. (2006). The optical properties of sputtered composite of Al-AlN. *Solar Energy Materials and Solar Cells 90*, 1861-1874. https://doi.org/10.1016/j.solmat.2005.11.006